Gamow-Teller Transition Strengths from ^{56}Ni

M. Sasano,[1,2] G. Perdikakis,[1,2] R. G. T. Zegers,[1,2,3] Sam M. Austin,[1,2] D. Bazin,[1] B. A. Brown,[1,2,3] C. Caesar,[4] A. L. Cole,[5] J. M. Deaven,[1,2,3] N. Ferrante,[6] C. J. Guess,[7,2] G. W. Hitt,[8] R. Meharchand,[1,2,3] F. Montes,[1,2] J. Palardy,[6] A. Prinke,[1,2,3] L. A. Riley,[6] H. Sakai,[9] M. Scott,[1,2,3] A. Stolz,[1] L. Valdez,[1,2,3] and K. Yako[10]

[1]*National Superconducting Cyclotron Laboratory, Michigan State University, East Lansing, Michigan 48824-1321, USA*
[2]*Joint Institute for Nuclear Astrophysics, Michigan State University, East Lansing, Michigan 48824, USA*
[3]*Department of Physics and Astronomy, Michigan State University, East Lansing, Michigan 48824, USA*
[4]*GSI Darmstadt, Helmholtz-Zentrum für Schwerionenforschung, D-64291, Darmstadt, Germany*
[5]*Physics Department, Kalamazoo College, Kalamazoo, Michigan 49006, USA*
[6]*Department of Physics and Astronomy, Ursinus College, Collegeville, Pennsylvania 19426, USA*
[7]*Department of Physics, University of Massachusetts Lowell, Lowell, Massachusetts 01854, USA*
[8]*Khalifa University of Science, Technology & Research, 127788 Abu Dhabi, United Arab Emirates*
[9]*RIKEN Nishina Center, Wako, 351-0198, Japan*
[10]*Department of Physics, University of Tokyo, Tokyo, 113-0033, Japan*

(Received 2 August 2011; published 7 November 2011; publisher error corrected 19 December 2011)

A new technique to measure (p, n) charge-exchange reactions in inverse kinematics at intermediate energies on unstable isotopes was successfully developed and used to study the ^{56}Ni(p, n) reaction at 110 MeV/u. Gamow-Teller transition strengths from ^{56}Ni leading to ^{56}Cu were obtained and compared with shell-model predictions in the pf shell using the KB3G and GXPF1A interactions. The calculations with the GXPF1A interaction reproduce the experimental strength distribution much better than the calculations that employed the KB3G interaction, indicating deficiencies in the spin-orbit and proton-neutron residual potentials for the latter. The results are important for improving the description of electron-capture rates on nuclei in the iron region, which are important for modeling the late evolution of core-collapse and thermonuclear supernovae.

DOI: 10.1103/PhysRevLett.107.202501 PACS numbers: 21.60.Cs, 25.40.Kv, 25.60.Lg, 26.30.Jk

Electron capture (EC) and β decay on medium-heavy nuclei play important roles in late stellar evolution [1]. In core-collapse (type II) supernovae, these weak reactions strongly affect the evolution towards the explosion [2,3]. EC on ^{56}Ni is an important contributor to the change in the electron-to-baryon ratio in the core-collapse supernovae of stars of 25–40 solar masses [4]. Accurate EC rates on isotopes in the region near ^{56}Ni are also critical to better understand the nature of thermonuclear supernovae (type Ia) [5] and help constrain the explosion models [6].

Gamow-Teller (GT; $\Delta L = 0$, $\Delta S = 1$, $\Delta T_z = \pm 1$) transition strengths are the key ingredients for calculating EC rates. In this work, we extract the GT strengths from ^{56}Ni in the $\Delta T_z = -1$ (β^-) direction using the ^{56}Ni(p, n) reaction at 110 MeV/u in inverse kinematics. Because isospin-symmetry-breaking effects are small, the extracted strengths also describe GT transitions to ^{56}Co in the $\Delta T_z = +1$ (β^+/EC) direction and directly impact the EC rate estimates for the abovementioned astrophysical processes. More important is that the results provide a deeper insight into the validity of shell-model calculations used to generate strength distributions for many iron-group nuclei for which data are not available.

In the independent particle model, ^{56}Ni with $N = Z = 28$ is doubly magic. However, since both protons and neutrons occupy the same major (pf) shell, the proton-neutron interaction is relatively strong, thereby softening the $f_{7/2}$ core [7,8]. Shell-model calculations with the KB [9,10] and GXPF1 [11,12] families of interactions both predict that the probability of a closed $(f_{7/2})^{16}$ shell configuration for ^{56}Ni is about 65%. However, GT strengths calculated with the KB family of interactions, which have been used in the generation of a weak-reaction rate library for astrophysical calculations [13], differ drastically [14] from those using the GXPF1 family. The differences between the two sets of calculations impact the estimates for EC rates on ^{56}Ni by as much as 30% [14]. Moreover, by resolving the ambiguity between the two shell-model calculations for the case of ^{56}Ni, it becomes possible to improve the EC rate estimates for many nuclei in the iron group, which leads to an overall improvement of the input for the astrophysical simulations.

Charge-exchange (CE) reactions at intermediate energies ($E \gtrsim 100$ MeV/u) have been used extensively to investigate isovector excitations, and, in particular, to extract GT strength distributions [15]. The need to benchmark weak-reaction rates on isotopes in the pf shell of importance for stellar evolution has motivated many experiments on stable nuclei. However, the development of experimental techniques to study charge-exchange reactions on unstable isotopes has been a challenge; successful experiments have focused on the study of relatively light nuclei at low excitation energies (see, e.g., [16–18]). In this Letter, a new technique for performing (p, n) experiments with

unstable isotopes of any mass and up to high excitation energies is presented. The low-energy recoil neutron produced in the inverse (p, n) reaction is used to reconstruct the excitation energy (E_x) and scattering angle in the center-of-mass (c.m.) frame ($\theta_{\mathrm{c.m.}}$); the detection of the heavy residue (here, ^{56}Cu) or one of its decay products is used to tag the CE reaction.

A 20-pnA, 160 MeV/u beam of ^{58}Ni from the NSCL Coupled Cyclotron Facility struck a 410-mg/cm^2-thick Be production target at the entrance of the A1900 fragment separator [19]. The secondary beam was purified by placing a 237-mg/cm^2-thick aluminum wedge at the intermediate image and a momentum-defining slit at the A1900 focal plane. The resulting cocktail beam of $N = 28$ isotones, with a momentum spread of $\pm 0.25\%$, had an intensity of $\sim 8 \times 10^5$ pps and contained ^{56}Ni at 110 MeV/u (66%), ^{55}Co at 106 MeV/u (32%), and ^{54}Fe (2%) at 102 MeV/u. The beam energies were obtained by injecting the beams into the spectrograph and measuring their momenta. The beam was transported to a liquid hydrogen target placed 65 cm upstream of the pivot point of the S800 spectrograph [20]. The target had an average thickness of 60 mg/cm^2 and was contained by 125-μm-thick Kapton foils. The time of flight (TOF) between an in-beam diamond detector [21] placed upstream of the target and a plastic scintillator placed in the focal plane of the spectrograph uniquely labeled the isotopes in the cocktail beam. The TOF measurement was combined with the energy loss measurement in an ionization chamber to perform the particle identification (PID) of the heavy residues. PID plots for events generated by ^{56}Ni and ^{55}Co beams are shown in Figs. 1(a) and 1(b), respectively. PID gates in these plots were used to select residual particles in the spectrograph. The two-dimensional widths of these gates varied between 1σ and 2σ to reduce the contamination from neighboring isotopes to insignificant levels.

Recoil neutrons from the (p, n) reaction were detected in the newly constructed Low-Energy Neutron Detector Array (LENDA) [22], consisting of 24 plastic scintillators bars placed at beam height and at 1 m from the target. Each bar had a vertical height of 300 mm ($\Delta\phi = \pm 8.5°$), a depth along the axis through the target of 25 mm, and a width of 45 mm ($\Delta\theta = \pm 2.6°$). Laboratory angles between 20° and 70° were covered, with gaps of 1.7° between bars. High-gain photomultiplier tubes were attached to both ends of each bar. The time reference for the neutron TOF measurement, from which the neutron energy was deduced, was provided by the abovementioned in-beam diamond detector. The neutron TOF resolution was 700 ps. The light-output thresholds were set to 35 keV (electron equivalent). Neutron-detection efficiencies, ranging from 40% at $E_n = 0.3$ MeV to 20% at $E_n = 4.0$ MeV, were calculated using the simulation code MCNP [23]. The validity of the simulations was confirmed by comparing with measured efficiencies using a ^{252}Cf fission source [24].

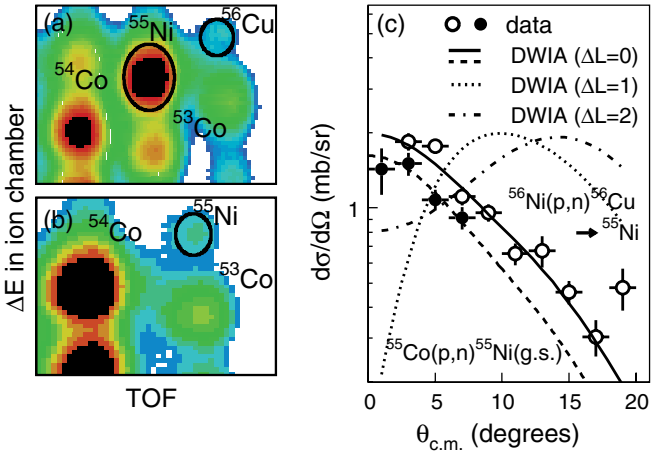

FIG. 1 (color online). PID spectra in the spectrograph for events associated with the (a) ^{56}Ni component and (b) ^{55}Co component in the beam. The event selections for ^{56}Ni, ^{55}Co(p, n) CE reactions used in the analysis are indicated by the ovals. (c) Differential cross sections for the ^{55}Co$(\frac{7}{2}^-, \mathrm{g.s.}) \times (p, n)^{55}Ni(\frac{7}{2}^-, \mathrm{g.s.})$ reaction and the ^{56}Ni$(p, n)^{56}$Cu reaction at $E_x(^{56}\mathrm{Cu}) = 4$–$4.5$ MeV. The angular range for the former transition is limited to $\theta_{\mathrm{c.m.}} < 8°$ by the acceptance of LENDA. In both cases, the angular distribution is well-reproduced by DWIA calculations, assuming $\Delta L = 0$ contributions only. For comparison, angular distributions associated with $\Delta L = 1$ and $\Delta L = 2$ are shown, as well.

Decay by proton emission of ^{56}Cu (proton-separation energy of 560 keV) to ^{55}Ni was dominant for $E_x(^{56}\mathrm{Cu}) > 1$ MeV. Above $E_x(^{56}\mathrm{Cu}) \approx 6$ MeV, decay by two subsequent proton emissions to ^{54}Co becomes energetically possible, but no significant contribution from this decay channel was observed below $E_x(^{56}\mathrm{Cu}) = 10$ MeV. Gamow-Teller transitions mainly populate states below that energy. Therefore, the present discussion focuses on events in which neutrons detected in LENDA were coincident with the detection of either ^{56}Cu or ^{55}Ni in the spectrograph. We also analyzed the ^{55}Co$(\frac{7}{2}^-, \mathrm{g.s.})(p, n)^{55}Ni(\frac{7}{2}^-, \mathrm{g.s.})$ reaction (^{55}Ni detected in the spectrograph). It is useful for calibration purposes, since the $\log ft = 3.6$ is known from β^+ decay [25].

Values of E_x and $\theta_{\mathrm{c.m.}}$ were reconstructed from the kinetic energy and laboratory scattering angles of neutrons detected in LENDA in coincidence with the residuals in the spectrograph. The excitation-energy resolution varied from 1 MeV at $\theta_{\mathrm{c.m.}} = 2°$ to 2.2 MeV at $\theta_{\mathrm{c.m.}} = 20°$. The uncertainty in $\theta_{\mathrm{c.m.}}$ was less than 0.5°. The data were grouped in excitation-energy bins of 0.5-MeV wide and center-of-mass scattering-angle bins of 2° wide and corrected for geometrical acceptances and neutron-detection efficiencies. Absolute differential cross sections were determined with an uncertainty of 10% by taking into account the efficiencies of the detectors and PID gates,

the transmission of the beam from the diamond detector to the target, and the dead time of the data acquisition system.

The ^{56}Ni$(p,n)^{56}$Cu $\rightarrow$ ^{55}Ni + p channel was contaminated by ^{56}Ni $\rightarrow$ ^{55}Ni + n knockout or fragmentation reactions. Such processes are not associated with the production of low-energy recoil neutrons, but with fast forward-peaked neutrons that could indirectly scatter from the surroundings into LENDA. The featureless shape of this background was found to be nearly independent of the reaction channel and was estimated by using ^{56}Ni $\rightarrow$ ^{53}Co + $2n + p$ events, since ^{53}Co cannot be created in the decay of ^{56}Cu excited to energies under consideration. The modeled background was scaled to match the spectra containing the CE events for unphysical values for E_x. The uncertainty in this subtraction procedure was the largest source of systematic errors in the analysis ($\sim 15\%$).

The GT strength [B(GT)] can be extracted from the data by using the well-established proportionality between the $\Delta L = 0$ cross section at 0° [$\sigma_{\Delta L=0}(0°)$] and B(GT) [26]:

$$\sigma_{\Delta L=0}(0°) = \hat{\sigma}_{\rm GT} F(q,\omega) B({\rm GT})/f_{\rm GT}, \qquad (1)$$

where $\hat{\sigma}_{\rm GT}$ is the GT unit cross section and $F(q,\omega)$ represents the dependence of $\sigma_{\Delta L=0}$ on the momentum (q) and energy (ω) transfers. For a pure GT transition, $f_{\rm GT} = 1$, and, for a transition that has both GT and Fermi ($\Delta L = 0$, $\Delta S = 0$) components, $f_{\rm GT} < 1$. For Fermi transitions, a proportionality similar to Eq. (1) exists, but with a different unit cross section $\hat{\sigma}_{\rm F}$. The GT unit cross section was calibrated using the ^{55}Co($\frac{7}{2}$, g.s.)$(p,n)^{55}$Ni($\frac{7}{2}$, g.s.) excitation, for which the measured differential cross sections are shown in Fig. 1(c). The value of $f_{\rm GT} = 0.51 \pm 0.03$ for this transition was established by using the known Fermi [$B(F) = N - Z = 1$] and GT {B(GT) = 0.267 [27]} strengths and the ratio $R^2 = \frac{\hat{\sigma}_{\rm GT}}{\hat{\sigma}_F} = 4.0 \pm 0.2$, which was derived from its well-established beam energy dependence [26]. The values of $F(q,\omega)$ for the Fermi and GT contributions were determined in the distorted-wave impulse approximation (DWIA; see below) and differed by less than 1%. $\sigma_{\Delta L=0}(0°)$ was extracted from the data by fitting the calculated differential cross sections in DWIA [also shown in Fig. 1(c)] to the experimental cross sections. By using Eq. (1), we found that $\hat{\sigma}_{\rm GT} = 3.2 \pm 0.5$ mb/sr, which is consistent with the value of 3.5 ± 0.2 mb/sr reported for the ^{58}Ni(p,n) reaction at 120 MeV [26].

To apply Eq. (1) to the ^{56}Ni(p,n) data, the forward-peaking $\Delta L = 0$ contributions to the full excitation-energy spectrum must be isolated from contributions with $\Delta L > 0$, whose angular distributions do not peak at 0°. This was done by performing a multipole decomposition analysis (MDA) [28,29] in which the angular distribution for each bin in $E_x(^{56}$Cu) was fitted with a linear combination of calculated angular distributions in DWIA with $\Delta L = 0$, 1, and 2. The inclusion of additional components with $\Delta L > 2$ did not improve the quality of the fits. Because the resolution in E_x deteriorated with increasing angle, the spectra at forward angles were smeared with Gaussian line shapes to avoid artificial biases in the MDA. The DWIA calculations were performed with the code DW81 [30], in conjunction with the effective interaction at 140 MeV from Ref. [31] and optical potentials from Ref. [32]. A normal-modes procedure [33] was used to generate the transition densities, which can be regarded as an average over all possible $1p - 1h$ contributions.

In Figs. 2(a)–2(d), the results of the MDA are shown for spectra at two scattering angles and separately for events associated with the detection of ^{56}Cu and ^{55}Ni in the spectrograph. Also shown in Fig. 2(e) is the spectrum at forward scattering angles, but without the smearing applied to account for the deterioration of the resolution at larger scattering angles as described above. Two peaks at 3 and 5 MeV can clearly be seen. The MDA shown in Figs. 2(c) and 2(d) indicates that 95% of the yield for $1 < E_x(^{56}{\rm Cu}) < 6$ MeV is due to $\Delta L = 0$ GT transitions. Above 6 MeV, dipole transitions dominate. Below the proton-decay threshold [Figs. 2(a) and 2(b)], no significant GT strength is found, and the response is dominated by transitions with $\Delta L = 2$.

Equation (1) was then applied to the extracted values of $\sigma_{\Delta L=0}$, with the unit cross section determined from the

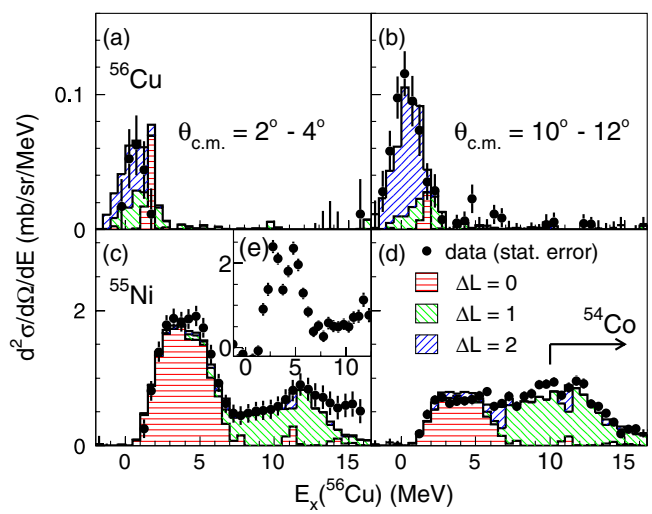

FIG. 2 (color online). Differential cross sections and the MDA of the ^{56}Ni$(p,n)^{56}$Cu* data. Results are presented for (a), (c) $\theta_{\rm c.m.} = 2° - 4°$ and (b),(d) $\theta_{\rm c.m.} = 10° - 12°$. The spectra are shown separately for (a),(b) events in which ^{56}Cu does not decay by proton emission and is detected in the focal plane of the spectrograph and for (c),(d) events in which ^{56}Cu decays by proton emission and ^{55}Ni is detected in the spectrograph. Above 10 MeV, events associated with the detection of ^{54}Co in the spectrograph (due to two decays by proton emission from ^{56}Cu) contribute. This energy is indicated by an arrow in (d), but these events are not included in the figures. (e) shows the spectrum measured at $\theta_{\rm c.m.} = 2° - 4°$ without the artificial smearing applied to the data in (c) (see text for details). Two peaks at $E_x(^{56}{\rm Cu}) = 3$ and 5 MeV are clearly visible in this spectrum.

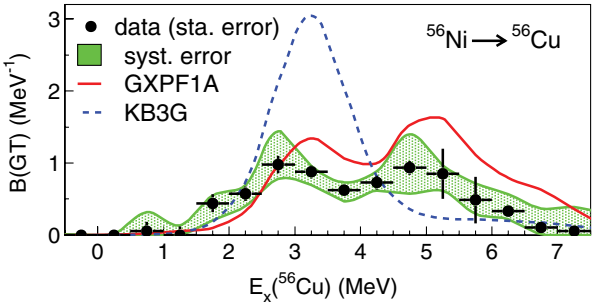

FIG. 3 (color online). Extracted GT strength distribution in ^{56}Cu and the comparison with shell-model calculations using the KB3G and GXPF1A interactions. The indicated systematic error band does not include the uncertainty in the absolute value of the GT unit cross section. Statistical errors are dominated by the uncertainties in the MDA fitting and, for some data points, are smaller than the markers.

^{55}Co data. The extracted GT strengths from the spectra associated with ^{56}Cu and ^{55}Ni residuals were then combined in a single strength distribution, as shown in Fig. 3. Because nearly all the yield at $1 < E_x(^{56}\mathrm{Cu}) < 6$ MeV was due to GT transitions, the unsmeared distribution shown in Fig. 2(e) was used in the determination of the final strength distribution, corrected for the small contributions ($\sim 5\%$) from other multipolarities extracted in the MDA. The systematic errors (shaded band in Fig. 3) are dominated by the uncertainties in the background subtraction, the input parameters of the DWIA calculations, and the smearing procedure. The uncertainty of 15% in $\hat{\sigma}_{\mathrm{GT}}$ is not included in this band.

Also shown in Fig. 3 are shell-model calculations [34] performed in the full pf shell, using the KB3G [10] and GXPF1A [12] interactions, which have been smeared with the experimental resolution. Following Ref. [35], both strengths have been scaled by a quenching factor $(0.74)^2$, associated with degrees of freedom that cannot be included in the shell-model theory. Except for a shift of about 0.5 MeV, the calculations with the GXPF1A interaction match the shape of the experimental strength distribution quite well. In contrast, the calculation with the KB3G interaction predicts that a large fraction of the strength is concentrated in a single state at 3 MeV. In both calculations, the GT strength is dominated by contributions from $f_{7/2} - f_{5/2}$ $1p - 1h$ excitations. However, due to weaker spin-orbit and residual proton-neutron potentials in the case of the KB3G interaction, the average excitation energy for GT transitions is lower by about 1.5 MeV compared to the GXPF1A interaction. Since the level density rapidly increases with increasing excitation energy, the spreading of the strength is enhanced in the case of the GXPF1A interaction, resulting in a broadening of the strength distribution. The effect is enhanced by the fact that the predicted level densities for 1^+ states with the GXPF1A interaction were about double those predicted with KB3G for $E_x(^{56}\mathrm{Cu}) < 7$ MeV. The integrated GT strengths for $E_x(^{56}\mathrm{Cu}) < 7$ MeV predicted in the theory $[\Sigma B(\mathrm{GT}) = 5.53(5.23)$ for GXPF1A (KB3G)] are slightly higher than those extracted from the data $[\Sigma B(\mathrm{GT})_{\mathrm{exp}} = 3.5 \pm 0.3(\mathrm{stat}) \pm 1.0(\mathrm{syst})]$. However, given the additional uncertainty in $\hat{\sigma}_{\mathrm{GT}}$, it is not possible to determine whether these differences are significant.

In summary, we have developed a new method to perform (p, n) charge-exchange experiments at intermediate energies in inverse kinematics, which enables the study of isovector excitations in unstable isotopes over large excitation-energy ranges. The method was successfully applied to the extraction of Gamow-Teller transition strength from the astrophysically important nucleus ^{56}Ni. Shell-model calculations with the KB3G interaction, which is a slightly improved version of the interaction used for creating the most comprehensive weak-rate library available, do not reproduce the data. Calculations with the GXPF1A interactions match the data better. The relatively weak spin-orbit and residual proton-neutron interactions in case of the calculation with the KB3G interaction were identified as the main cause for the discrepancy between these calculations and the data.

We thank the staff at NSCL for their support. This work was supported by the US NSF (Grants No. PHY-0822648 (JINA), No. PHY-0606007, No. PHY-0758099, No. PHY-0922615, and No. PHY-1068217), the US DOE (Grant No. DE-FG02-94ER40848), and the Research Corporation of Science Advancement.

[1] K. Langanke and G. Martínez-Pinedo, Rev. Mod. Phys. **75**, 819 (2003) and references therein.
[2] A. Heger, S. E. Woosley, G. Martínez-Pinedo, and K. Langanke, Astrophys. J. **560**, 307 (2001).
[3] W. R. Hix *et al.*, Phys. Rev. Lett. **91**, 201102 (2003).
[4] A. Heger, K. Langanke, G. Martínez-Pinedo, and S. E. Woosley, Phys. Rev. Lett. **86**, 1678 (2001).
[5] F. Brachwitz *et al.*, Astrophys. J. **536**, 934 (2000).
[6] K. Iwamoto *et al.*, Astrophys. J. Suppl. Ser. **125**, 439 (1999).
[7] A. F. Lisetskiy *et al.*, Phys. Rev. C **68**, 034316 (2003).
[8] K. Minamisono *et al.*, Phys. Rev. Lett. **96**, 102501 (2006).
[9] E. Caurier, F. Nowacki, A. Poves, and J. Retamosa, Nucl. Phys. **A654**, 973c (1999).
[10] A. Poves, J. Sánchez-Solano, E. Caurier, and F. Nowacki, Nucl. Phys. **A694**, 157 (2001).
[11] M. Honma, T. Otsuka, B. A. Brown, and T. Mizusaki, Phys. Rev. C **69**, 034335 (2004).
[12] M. Honma *et al.*, J. Phys. Conf. Ser. **20**, 7 (2005).
[13] K. Langanke and G. Martínez-Pinedo, At. Data Nucl. Data Tables **79**, 1 (2001).
[14] T. Suzuki, M. Honma, H. Mao, T. Otsuka, and T. Kajino, Phys. Rev. C **83**, 044619 (2011).
[15] F. Osterfeld, Rev. Mod. Phys. **64**, 491 (1992).
[16] T. Nakamura *et al.*, Phys. Lett. B **493**, 209 (2000).
[17] R. G. T. Zegers *et al.*, Phys. Rev. Lett. **104**, 212504 (2010).
[18] Y. Satou *et al.*, Phys. Lett. B **697**, 459 (2011).

[19] D. Morrissey *et al.*, Nucl. Instrum. Methods Phys. Res., Sect. B **204**, 90 (2003).
[20] D. Bazin *et al.*, Nucl. Instrum. Methods Phys. Res., Sect. B **204**, 629 (2003).
[21] A. Stolz, M. Behravan, M. Regmi, and B. Golding, Diam. Relat. Mater. **15**, 807 (2006).
[22] G. Perdikakis *et al.*, IEEE Trans. Nucl. Sci. **56**, 1174 (2009).
[23] Monte Carlo NParticle Transport Code System, MCNP5-1.60 and MCNPX-2.7.0, http://www-rsicc.ornl.gov/codes/ccc/ccc7/ccc-740.html.
[24] W. Mannhart, in *Proceedings of a Consultants' Meeting on Physics of Neutron Emission in Fission, Mito City, Japan, 1988*, edited by H. D. Lemmel (IAEA Nuclear Data Section, Vienna, 1989), p. 305.
[25] H. Junde, Nucl. Data Sheets **109**, 787 (2008).
[26] T. N. Taddeucci *et al.*, Nucl. Phys. **A469**, 125 (1987).
[27] J. Äystö *et al.*, Phys. Lett. **138B**, 369 (1984).
[28] B. Bonin *et al.*, Nucl. Phys. **A430**, 349 (1984).
[29] T. Wakasa *et al.*, Phys. Rev. C **55**, 2909 (1997).
[30] R. Schaeffer and J. Raynal, Program DWBA70 (unpublished); J. R. Comfort, Extended Version DW81 (unpublished).
[31] M. A. Franey and W. G. Love, Phys. Rev. C **31**, 488 (1985).
[32] A. Nadasen *et al.*, Phys. Rev. C **23**, 1023 (1981).
[33] M. A. Hofstee *et al.*, Nucl. Phys. **A588**, 729 (1995).
[34] B. A. Brown, W. D. M. Rae, E. McDonald, and M. Horoi, NuShellX@MSU, http://www.nscl.msu.edu/brown/resources/resources.html.
[35] G. Martínez-Pinedo, A. Poves, E. Caurier, and A. P. Zuker, Phys. Rev. C **53**, R2602 (1996).